Journal of Ceramic Processing Research. Vol. 24, No. 3, pp. 541~553 (2023)
(Received 24 February 2023, Received in revised form 9 April 2023, Accepted 24 April 2023)
https://doi.org/10.36410/jcpr.2023.24.3.541

J O U R N A L O F
Ceramic Processing Research

Study of dry friction characteristics of silicon nitride full ceramic ball bearing with PEEK-based cage

Jian Sun[a,b], Zhe Zhang[a], Zhongxian Xia[a], Xin Fang[a], Renyun Guan[a], Guangxiang Zhang[a] and Jinmei Yao[a,*]
[a]*School of Mechanical Engineering, Shenyang Jianzhu University, Shenyang 110168, China*
[b]*State Key Laboratory of Tribology, Tsinghua University, Beijing 100084, China*

In order to investigate the influence of polyether ether ketone (PEEK) and its composite cage on the dry friction characteristics of silicon nitride all-ceramic ball bearings, this paper firstly conducted a theoretical analysis of silicon nitride deep groove ball bearings subjected to radial load under dry friction conditions, and then conducted dry friction tests and simulation studies on PEEK, CF30 and PVX cage silicon nitride full ceramic ball bearings. The test results show that the temperature rise of CF30 and PVX cage bearings is higher than that of PEEK cage bearings; the relationship between the root mean square value of vibration of PEEK, CF30 and PVX cage bearings is PEEK cage bearings > CF30 cage bearings > PVX cage bearings; the simulation model has good accuracy; Surface morphology analysis of the PVX cage bearing after the test show that the transfer film has the effect of wear reduction and lubrication on the bearing. The results of the study have positive significance for the research of transfer film lubricated bearings and the selection of cage materials.

Keywords: PEEK-based cage, Full ceramic ball bearings, Transfer film, Dry friction.

Introduction

Silicon nitride full ceramic ball bearings have long life, wear resistance, corrosion resistance, high temperature, and low-temperature resistance, non-permeability, and other excellent performance of the traditional steel bearings do not have [1, 2], even so, silicon nitride full ceramic ball bearings in dry friction and extreme working conditions will still wear, which will affect its service life and accuracy, and in aerospace and other high-precision fields, does not allow the existence of oil vapor pollution, new solid lubrication, and oil-free lubrication will replace oil lubrication [3]. Therefore it is particularly important to use solid lubricated bearings with self-lubricating performance cages.

Because PEEK engineering plastics have good self-lubricating properties, friction resistance, corrosion resistance, high-temperature stability, and aging resistance [5], widely used as a matrix for polymer materials and then applied to bearings as a cage material, PEEK has higher hardness and wear resistance through the addition of modified materials. Under dry friction conditions in bearings, these polymer materials form a transfer film on the bearing grooves and rolling element surfaces to provide wear reduction and lubrication. Many scholars have done extensive research on the tribological properties of PEEK and its composites. Placette M.D. et al. [6] investigated the mechanism of PEEK transfer film development during reciprocating motion and showed that a thin and continuous transfer film corresponds to less wear and that frictional heat plays a key role in the PEEK transfer film mechanism and can influence the volume and development of the transfer film. Qi Y. et al. [7] investigated the tribological behavior of PTFE filled with PEEK and Nano-ZrO_2 and found that the PTFE composites with 10% PEEK and 8% Nano-ZrO_2 additions had the best wear resistance as well as the addition of nanomaterials facilitated the formation of transfer films. Wang A. et al. [8] investigated the aqueous phase lubrication between PEEK and Si_3N_4 friction subsets and showed that water accelerated the formation of transfer film and the underwater wear rate of PEEK- Si_3N_4 friction subsets was about more than twice the dry sliding wear rate. Ma J. et al. [9] found that the mechanism of transfer film formation in PI/MPS nanocomposites during dry sliding against bearing steel is the tribochemical adhesion of abrasive chips and their subsequent accumulation, which is the result of the combined effect of tribochemical and abrasive chip size reduction and morphological changes. Guo L et al. [10] investigated the effect of nanocomposite particles on the tribological properties and tribological film function of PEEK, where the combination of WS_2-silicon carbide nanoparticles produced a "smooth" tribological film with poor wear resistance. The hard particles give the friction film a high load-bearing

*Corresponding author:
Tel : +86-188 0982 2007
Fax: 024-24694985
E-mail: yaojinmei06@126.com

capacity, while the soft particles give the film easy shear properties. Theiler G et al. [11] investigated the friction and wear of PEEK composites in a vacuum environment and showed that the MoS_2-filled composites had a low coefficient of friction and wear rate at -80 ℃, which is related to the polymer transfer film on the surface, and in addition, the sliding speed has a significant effect on the friction and wear properties of MoS_2-filled PEEK. The best performance *pv* value at room temperature in vacuum is 1 MPa·m/s. Gao Jintang [12] also confirmed that the frictional wear properties of polymers are closely related to the adhesion strength and degree of coverage of the transfer film.

The above studies have confirmed the self-lubricating properties of polymers and their composite materials, but most of them only focus on the friction and wear of plane friction pairs, and there are relatively few studies on the actual operation of composite cages in rolling bearings, and the research on silicon nitride ceramic materials is also very important. Koike H et al. [13] investigated the wear of poly ether-ether-ketone (PEEK) hybrid radial ball bearing, they found the PEEK adhesion film including PTFE and graphite wear particles on the raceway of the bearing's inner ring during the test, the result showed that the PEEK-PTFE adhesion film improved dramatically wear and rotational performance of the bearing. Hyuga H et al. [14] studied the tribological behavior of single piece Si_3N_4 and Si_3N_4 based composite materials in the water environment. The results showed that due to the solid lubrication effect of the composite material, the friction coefficient of Si_3N_4-based composite material significantly decreased, and with the dispersion of solid lubricant, the running distance became shorter. Lu Y et al. [15] investigated the influences of alpha-Si_3N_4 seeds and sintering additives on the microstructure and mechanical properties of porous Si_3N_4 ceramics and found that the resultant porous Si_3N_4 ceramics had a fine microstructure and a uniform pore structure. With an increase in the alpha- Si_3N_4 seeds content, the porosity decreased, and the flexural strength increased accordingly. Ahn SH et al. [16] analyzed the elastic wave characteristics in the abrasion test of two types of Si_3N_4. The results showed that the friction coefficients vary with the amount of SiO_2 nano-colloid, and the heat treatment temperature, also the mechanical properties are determined by the components of the main ceramics in sintering. Xin H et al. [17] investigated the effects of sliding speed and contact load on the tribological performance of silicon nitride based bearing subsets. It was found that interfacial lubrication is achieved by the formation of a solid lubricating film and that the friction coefficient and wear rate decrease with increasing load or speed as well as the addition of hexagonal boron nitride affects the quality of the solid lubricating film. Xia Z et al. [18] studied silicon nitride ceramic bearings with self-lubricating materials as cages under extremely low temperature and heavy load conditions. The results show that a self-lubricating film is formed inside the bearing, and the Si_3N_4 ring and cage Conditions have better adaptability, but the cage is the weak link. Yakout et al. [19, 20] and Zaretsky et al. [21, 22] studied the relationship between internal clearance and the dynamic characteristics, vibration characteristics, and service life of rolling bearings. The results show that internal clearance has a significant influence on the dynamic characteristics and performance of rolling bearings. Fang B et al. [23] studied the variation law of the nonlinear stiffness of double row angular contact ball bearings (DR-ACBB), and found that it has nonlinear soft spring stiffness characteristics in the low speed range and light load conditions (that is, the stiffness varies with the outer The load decreases), while it has a nonlinear hard spring stiffness characteristic (that is, the stiffness increases with the external load) in the high-speed range or under heavy load conditions. Ma SJ et al. [24] proposed a dynamic model of the bearing-rotor system by introducing semi-flexible body elements (SFBE). And found that under eccentric excitation, the ball goes through at least two load zones per revolution. As the contact angle increases, the stability of the cage gets worse but then improves. Mingkai W et al. [25] established a comprehensive dynamic model of ball bearings focusing on structural flexible deformation, and the results showed that reasonable structural flexible design can optimize the rotational performance of the bearing. In addition, Wang J et al. [26] found through the simulation study of solid lubricating bearings that when the contact surface of the raceway with a solid lubricating coating comes into contact with the ball, the coating undergoes elastic deformation, the contact area increases and the contact stress decreases, which can effectively protect the bearing. In fact, the lubricating effect of the cage in the operation of the rolling bearing depends on the wear particles generated by its sliding motion with the balls [27, 31], so it is essentially particle lubrication. During the operation of the bearing, the cage first contacts the balls to form lubricating particles. These particles are transferred to the inner and outer ring grooves with the rotation and revolution of the balls, and some of them are attached to the surface of the balls. With the operation of the bearing, the particles are in contact. The points circulate continuously and are gradually compacted to form a transfer film. This process has the first transfer of lubricating particles from the cage to the balls and the second transfer of the balls to the inner and outer channels, so it is called double transfer lubrication.

During the transfer lubrication process, the cage plays a vital role. How to effectively control the wear of the cage so that the wear particles form a thin and uniform transfer film in the bearing is the focus of our

research, because it must be maintained throughout the life of the bearing There is a transfer film during the cycle. To achieve this, the material selection of the cage is very important. These self-lubricating materials must have low wear resistance, and PEEK polymers and their composite materials can meet this requirement. Therefore, this paper selects silicon nitride full ceramic ball bearings with three cage materials: PEEK, CF30, and PVX, and conducts dry friction experiments and simulation studies on them, it provides a basis for the study of the cage lubrication mechanism of silicon nitride full ceramic ball bearings and the selection of cage materials.

Mathematical model of self-lubricating silicon nitride full ceramic ball bearing

Stress and strain analysis of deep groove ball bearing under radial load

Figure 1 shows the deformation diagram of a deep groove ball bearing under radial load.

Figure 1(a) $\frac{1}{2}u$ indicates the radial clearance of the ball to the outer ring groove. When the bearing is subjected to radial load, a vertical displacement is generated.

$$\delta = \delta_{\max} + \frac{1}{2}u \tag{1}$$

Where, $\delta_{\max}$ is the maximum deformation of the bottom ball, according to the variability coordination condition, that is, the vertical displacement caused by the radial force is equal to the sum of the vector of the deformation of the ball at each angle, the deformation of the ball at any angle δ_φ is

$$\delta_\varphi = \delta_{\max}\left(1 - \frac{(1-\cos\varphi)\bullet(2\delta_{\max}+u)}{2\delta_{\max}}\right) \tag{2}$$

let

$$\varepsilon = \frac{1}{2}\left(\frac{2\delta_{\max}}{2\delta_{\max}+u}\right) \tag{3}$$

The equation (2) then becomes

$$\delta_\varphi = \delta_{\max}\left(1 - \frac{1-\cos\varphi}{2\varepsilon}\right) \tag{4}$$

When the bearing is subjected to radial load, there exists a limit angle φ_1 lets δ_φ be 0, at this time φ_1 is

$$\varphi_1 = \pm ar\cos\left(\frac{u}{2\delta_{\max}+u}\right) \tag{5}$$

From the above equation, we can see that the limit angle is $\varphi_1 < 180°$, that is, the range of the bearing area is less than 180°. According to the Hertzian contact theory, the relationship between the deformation of the load-bearing area and the contact load is

$$Q_j = K \cdot \delta_j^{\frac{3}{2}} \tag{6}$$

Where, Q_j denotes the contact load of the jth ball, K indicates the load-deformation coefficient, δ_j denotes the deformation of the jth roller ball. According to equation (6), it can be derived that

$$\frac{Q_\varphi}{Q_{\max}} = \left(\frac{\delta_\varphi}{\delta_{\max}}\right)^{\frac{3}{2}} \tag{7}$$

Where, Q_φ and $Q_{\max}$ indicates the contact load of the ball in φ position and bottom position, δ_φ and $\delta_{\max}$ indicates the deformation of the ball in φ position and bottom position. Therefore

$$Q_\varphi = Q_{\max}\left(1 - \frac{1-\cos\varphi}{2\varepsilon}\right)^{\frac{3}{2}} \tag{8}$$

The equation for balancing the bearing balls in the load area is

$$F_r = \sum_{-\varphi_1}^{+\varphi_1} Q_{\max}\left[1 - \frac{1}{2\varepsilon}(1-\cos\varphi)\right]\cos\varphi \tag{9}$$

The integration of equation (9) is in the form

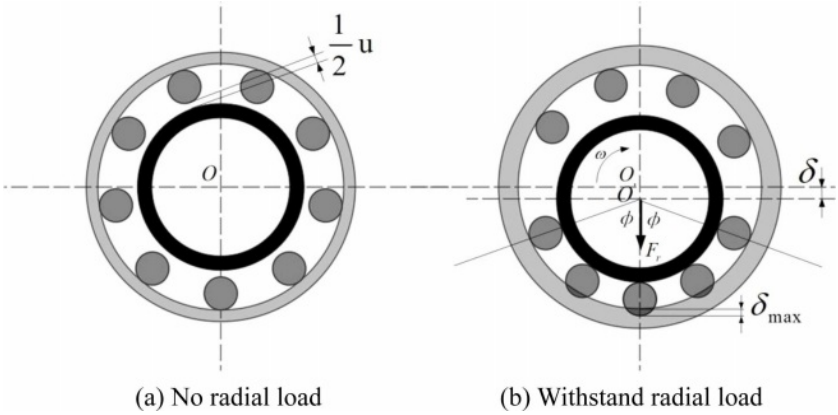

Fig. 1. Bearing mathematical model.

$$Q_{\max} = \frac{F_r}{Z \cdot J_r} \tag{10}$$

The maximum stress on the rolling element is

$$q_0 = \frac{3Q_{\max}}{2\pi ab} \tag{11}$$

Where, a is the semi-major axis of the ellipse contact area, b is the semi-minor axis of the ellipse contact area.

$$a = m_a \left[\frac{3Q_{\max}}{2\sum\rho} \left(\frac{1-\mu_1^{\ 2}}{E_1} + \frac{1-\mu_2^{\ 2}}{E_2} \right) \right]^{\frac{1}{3}} \tag{12}$$

$$b = m_b \left[\frac{3Q_{\max}}{2\sum\rho} \left(\frac{1-\mu_1^{\ 2}}{E_1} + \frac{1-\mu_2^{\ 2}}{E_2} \right) \right]^{\frac{1}{3}} \tag{13}$$

Where, m_a and m_b are the major and minor semi-axis coefficients, $\Sigma\rho$ is the summation of the principal curvature, μ is the Poisson's ratio, E is the modulus of elasticity. Note that when a transfer film is present, E_2 and μ_2 is the performance parameter of the transfer film material.

Substituting equation (10) into equation (8) yields

$$Q_\varphi = \frac{F_r}{Z \cdot J_r} \left(1 - \frac{1-\cos\varphi}{2\varepsilon} \right)^{\frac{3}{2}} \tag{14}$$

Analysis of friction torque of deep groove ball bearing under dry friction

Frictional torque is the main source of heat generation in bearings, which is mainly composed of the following components under dry friction conditions: elastic hysteresis, differential slip, rotational friction, and friction between balls and cages.

Friction torque caused by elastic hysteresis

When the ball rolls in the groove, an elastic hysteresis occurs as the strain lags behind the stress, resulting in resistance torque. Energy loss is [29]

$$E_j = 1.5\beta\Gamma \left| n - n_m \right| R \times \left(\frac{\pi\sum\rho}{2\zeta} \right)^{\frac{2}{3}} \cdot \left(\frac{1.5}{k} \right) \left(\frac{1-\varepsilon_1^2}{E_1} + \frac{1-\varepsilon_2^2}{E_2} \right)^{\frac{1}{3}} Q_\varphi^{\frac{4}{3}} \tag{15}$$

Where, β is the elastic hysteresis loss factor, silicon nitride ceramics are 0.0005. n and n_m are the rotational speeds of the bearing ring and the ball, E_1 and E_2 is the modulus of elasticity of the ball and bearing ring, k Indicates the ellipticity, R represents the distance between the point of contact and the axis of rotation of the ball, Γ and ζ denotes the first and second type of elliptic integrals. According to the law of conservation of energy, the friction torque due to the elastic hysteresis M_E is expressed as

$$M_E = \frac{\sum_{j=1}^{Z} E_j}{2\pi n} \tag{16}$$

Friction torque caused by differential slip

When a ball rolls with a certain radius in a planar groove perpendicular to the rolling direction, pure rolling occurs on the two straight lines of the contact ellipse, and on other parts of the ellipse, due to the unequal distance between the contact point and the axis of rotation, the ball will differential slip. The resulting energy loss is

$$E_{D,j} = \iint dE_D = \iint \frac{1.5 v_{\eta\xi} \mu_D F_j}{\pi a_j b_j} \left[1 - \left(\frac{\eta}{a_j} \right)^2 - \left(\frac{\xi}{b_j} \right)^2 \right]^{\frac{1}{2}} d\eta d\xi \tag{17}$$

Where, μ_D and $v_{\eta\xi}$ indicate the coefficient of friction between the ball and the raceway and the relative speed difference at which the ball and raceway slide over the contact area. According to the principle of energy conservation, the formula of friction torque caused by differential slip M_D is expressed as

$$M_D = \frac{\sum_{j=1}^{Z} E_j}{2\pi n} \tag{18}$$

Friction torque caused by rotational friction

When the center of the bearing inner ring is misaligned with the axis, friction occurs due to the rotation of the balls due to the angle θ between the centerline of the inner ring of the bearing and the horizontal. The friction torque generated by rotational friction can be expressed as

$$E_{S,j} = \frac{3F_j \omega_S a_j}{8} \times \int_0^{\frac{\pi}{2}} \mu_S \left\{ 1 - \left[\frac{1}{1 - \left(\frac{a_j}{b_j} \right)} \right] \sin^2\theta \right\}^{\frac{1}{2}} d\theta \tag{19}$$

Where, ω_S and μ_S indicates the rotational angular velocity of the ball as it rolls between the raceways and the rotational friction coefficient between the ball and the raceway. According to the principle of energy conservation, The formula for the friction torque M_S caused by rotational friction is expressed as

$$M_S = \frac{\sum_{j=1}^{Z} E_j}{2\pi n} \tag{20}$$

Friction torque caused by ball and cage friction

Under dry friction conditions, for bearings with self-lubricating cage, sliding friction is generated between the ball and the cage, and the abrasive chips generated by the collision and friction between the ball and the cage are sucked into the ball and the cage, impeding the movement of the ball. According to the principle of energy conservation, in the unit of time, the ball and cage cavity friction generated by the energy dissipation is equal to the bearing friction torque M_C generated by the energy loss, M_C is expressed as

$$M_C = \frac{\sum_{j=1}^{Z} E_j}{2\pi n} \tag{21}$$

Where, E_j is the sliding friction loss energy of the jth ball in unit time.

According to the above analysis, the expression of total friction torque of self-lubricating silicon nitride full ceramic deep groove ball bearing under dry friction condition is given

$$M = M_E + M_D + M_S + M_C \tag{22}$$

Test research

Test materials

In this experiment, P4 grade 6206 silicon nitride full ceramic deep groove ball bearings with clearance of C3 grade are used, which are made by a hot isostatic pressing sintering process. Table 1. lists its main structural parameters. For the cage material, three polymer materials, PEEK, CF30 (PEEK/30 wt%CF), and PVX (PEEK/10 wt%CF/10 wt%graphite/10 wt%PTFE), were selected, among which CF30 and PVX were made by Germany Available from Ensinger. Table 2. lists the physical properties of three polymer materials and Si_3N_4 ceramics.

Table 1. Structural parameters of 6206 deep groove ball bearings.

Structural parameters	Value
Bearing width	16 mm
Rolling element diameter	9.525 mm
Number of rolling elements	9
Bearing inner ring diameter	30 mm
Bearing outer ring diameter	62 mm

Test device

The test device used in this paper is ABLT-1A bearing life testing machine, as shown in Fig. 2(a), which consists of test head, test head base, transmission system, loading system, lubrication system, electrical control system, computer monitoring system and other parts. Fig. 2(b) shows the test shaft and bearings installed in the test head. The main technical indicators of the testing machine are: the inner diameter range of the test bearing is 10-60 mm; the number of test bearings: 2 sets or 4 sets; the range of radial load and axial load is 0-100 kN and 0-50 kN; the maximum rotation speed is 24000 r/min.

Test methods

Using the ABLT-1A bearing life testing machine, a single-factor dry friction test was carried out on PEEK, PVX and CF30 three types of cage bearings in an oil-free state. The test scheme is shown in Table 3.

Test results and analysis

Bearing temperature rise characteristics under dry friction conditions

In the dry friction experiment, the surface temperature of the outer ring of PEEK, PVX and CF30 cage bearings was measured by contact temperature sensors, and the radial load was varied at a speed n of 8000 r/min, and the speed was varied at a radial load Fr of 900N, and the test results are shown in Fig. 3.

From Fig. 3(b), we can see that the temperature rise of three kinds of cage bearings is proportional to the rotational speed, while Fig. 3(a) shows that the radial load has little effect on the temperature rise and even a slight decrease. The influence of rotational speed on the bearing is mainly reflected in the centrifugal force, the higher the rotational speed, the greater the centrifugal force, and the greater the contact load between the bearing ball and the outer ring, while accelerating the contact frequency between the ball and the inner and outer ring, so that the heat generated by friction increases,

Table 2. Physical properties of Si_3N_4, PTFE, PEEK, CF30 and PVX.

Parameters	Si_3N_4	PEEK	CF30	PVX
Density ρ/(g·cm^3)	3.3	1.35	1.38	1.44
Modulus of elasticity E/GPa	320	3.8	6	5.5
Poisson's ratio	0.26	0.4	0.47	0.1
Thermal conductivity W/m·K	20	0.25	0.66	0.82
Expansion coefficient 10^{-6}/K	3.1	22	40	30
Hardness	1520	210	298	250
Specific heat capacity J/(g*K)		1.3	1.2	1.1

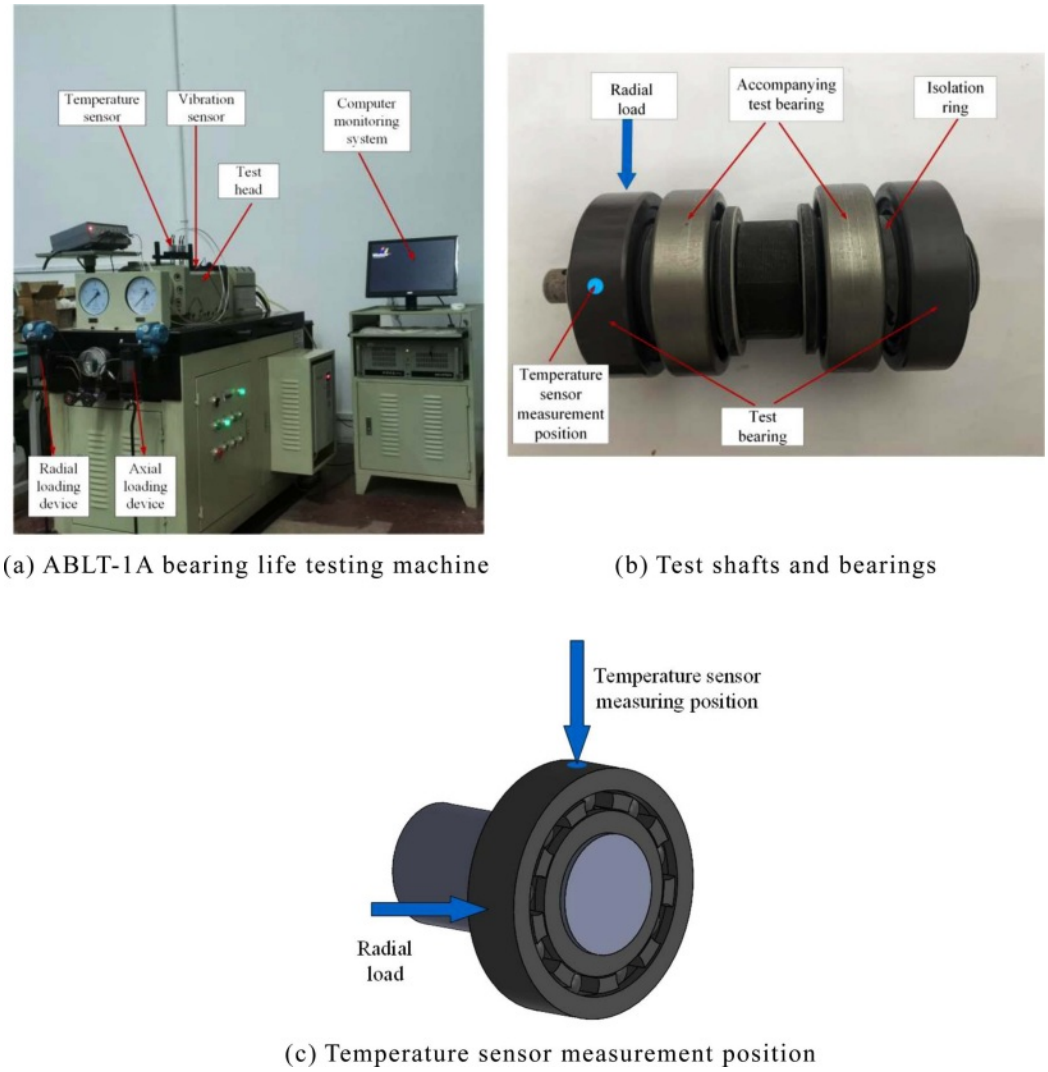

(a) ABLT-1A bearing life testing machine

(b) Test shafts and bearings

(c) Temperature sensor measurement position

Fig. 2. ABLT-1A bearing life testing machine, test shaft structure and temperature sensor measurement position.

Table 3. 6206 full ceramic ball bearing dry friction test conditions.

Cage type	Radial Load (N)	Contact load (GPa) Outer ring	Inner ring	Rotational Speed (r/min)	Test time
PEEK	400	1.65	1.54	4000	500 min
PVX	900	2.16	2.02	6000	
CF30	1750	2.70	2.52	8000	
	3000	3.23	3.01	10000	
	4750	3.76	3.51	12000	

and the temperature rise increases accordingly. On the other hand, the higher the speed, the greater the relative sliding speed difference v between the ball and the raceway on the elliptical contact area, so by the formula (18) and (19) can be seen, the differential slip caused by the friction torque M_D increased; In addition, the higher the speed, the ball in the vertical normal plane, the greater the rotational component, by the formula (20) and (21) can be seen, rotational friction caused by the friction torque M_S increased, bearing mechanical energy keeps rising and the temperature rise increases.

When the bearing is subjected to radial load, as can be seen from the formula (5), there is a limit angle φ_1 so that the ball is loaded to 0, in the limit angle that is the loading area, in the loading area, as can be seen from the formula (10) bearing ball contact load with the inner and outer ring increases with the increase of radial force, the contact area also increases; it is worth noting that, due to the ABLT-1A testing machine

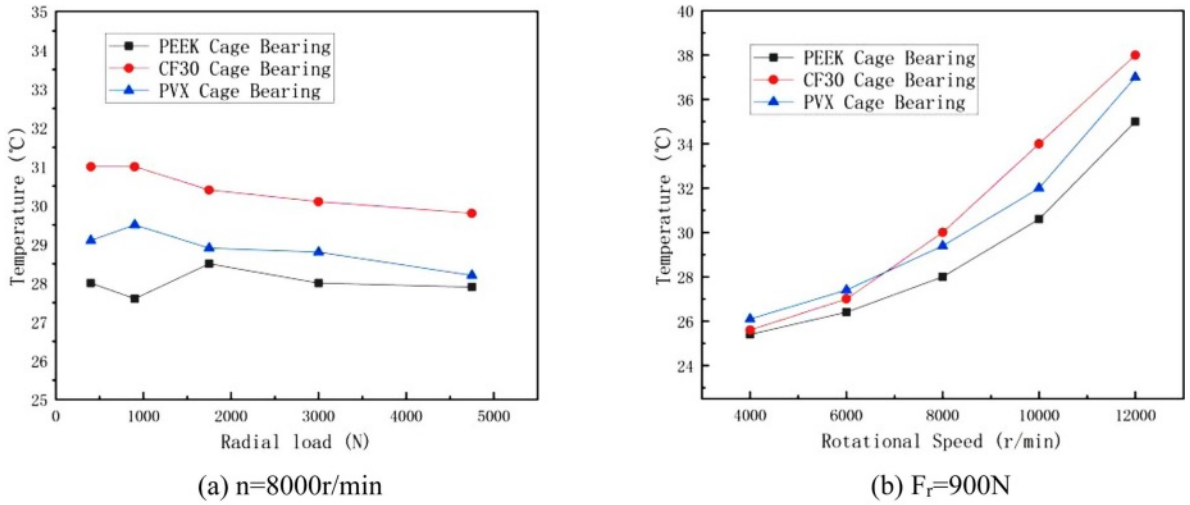

Fig. 3. Temperature rise of PEEK, CF30, PVX cage bearing under variable working conditions of dry friction.

temperature sensor measurement position is located in the bearing non-loading area, in the non-loading area, ball contact load is not affected by the change of radial force, but the ball is also affected by the centrifugal force, so that the radial load has little effect on the change of the temperature rise at the measurement point, or shows an inverse relationship.

At the same time, we observed from the test results that the temperature rise of the three bearings is ranked from high to low: CF30 cage bearings, PVX cage bearings, and PEEK cage bearings. The reason for this phenomenon is that during the bearing operation of the CF30 and PVX cages, due to collision and friction, the tiny particles on the composite material cages peel off, and after a double transfer process, a thin transfer film is formed on the inner and outer ring grooves and balls. Since the transfer film covers the contact surface of the bearing, and the pure PEEK cage is not filled with other materials, it is difficult to form an effective transfer film on the groove and the ball. The material of the transfer film is soft, and the shear viscous resistance between the ball and the raceway is large, that is, the frictional resistance of viscosity increases, so from the formulas (15) and (16), it can be seen that the friction torque M_E caused by the elastic hysteresis of the CF30 and PVX cage bearings is greater than the friction torque M_E caused by the elastic hysteresis of the PEEK cage bearings, and the formula (21) shows that the formation of the transfer film also causes the friction torque M_C between the ball and the pocket of the cage increases, and the total friction torque increases, which increases the heat generation of the bearing. On the other hand, the thermal conductivity of the transfer film and the heat transfer coefficient of the film layer are much lower than that of silicon nitride ceramics, which makes it difficult for the heat generated inside the bearing to dissipate. In summary, the temperature rise of CF30 and PVX cage bearings is slightly higher than that of PEEK cage bearings. PVX is based on PEEK, filled with PTFE, carbon fiber and graphite. Graphite has excellent lubricity. Based on ensuring strength, the synergistic effect of PTFE and PEEK is more conducive to the lubrication of bearings [30, 31]; while CF30 filled with carbon fiber,compared with PVX, although its strength is higher, its lubrication performance and heat dissipation are poor, so the temperature rise of CF30 cage bearings is higher than that of PVX.

Bearing vibration characteristics under dry friction

The root mean square value of the bearing vibration signal is related to the irregular vibration caused by bearing wear, which occurs mainly between the bearing ball and raceway, and the magnitude of the vibration value can well reflect the bearing wear. Its calculation formula is

$$X_S = \sqrt{\frac{\sum_{i=1}^{N} x_i^2}{N}} \tag{23}$$

Where, X_S is the root mean square value of the vibration, x_i is the sample value, N is the number of samples.

The vibration values of PEEK, PVX and CF30 cage bearings were measured by vibration sensors, and then the effective values were taken at different speeds and loads, and the test results are shown in Fig. 4. From the test results, it can be seen that the vibration values of the three bearings are proportional to the speed and load, and their root mean square values of vibration are PEEK cage bearing > CF30 cage bearing > PVX cage bearing. This is because of the poor adhesion of pure PEEK and silicon nitride ceramics, subject to shear, the PEEK film layer is destroyed, it is difficult to form an effective transfer film inside the bearing, resulting in

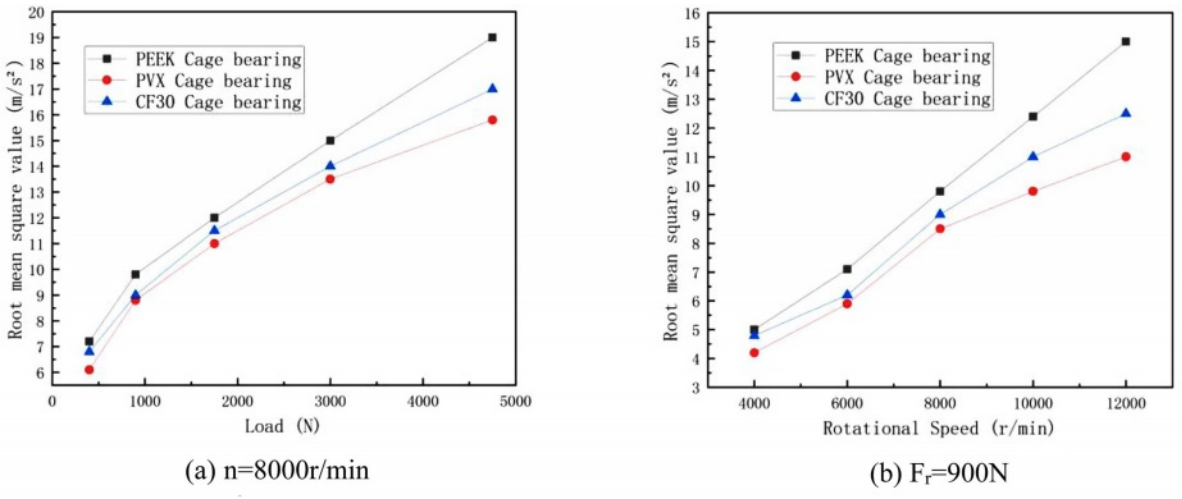

Fig. 4. Vibration of PEEK, CF30, PVX cage bearings under dry friction variable working conditions.

direct contact collision between the ball of silicon nitride material and the inner and outer grooves, the stress concentration is more obvious, which makes the vibration maximum. CF30 material is filled with only 30 wt% of carbon fiber, which improves the hardness and creep resistance of the substrate, but lacks the synergy of other materials and insufficient toughness of the transfer layer. In contrast, PVX material filled with PTFE, graphite, carbon fiber, carbon fiber is a rigid material, which improves the bearing capacity and anti-adhesion ability of the PEEK substrate, making it difficult to destroy the transfer film on the contact surface, which is conducive to the formation of a stable transfer film; graphite has excellent lubrication properties, reducing the coefficient of friction; PTFE is a laminar microstructure, its internal shear force is small, which is conducive to the transfer film PTFE is a layered microstructure with low internal shear force, which is conducive to the formation of transfer film, and also has a low friction coefficient. The effective transfer film separates the ball of silicon nitride bearing from the groove, and the soft contact replaces the hard contact, which is known from equation (11), the elastic modulus of the contacting object is reduced, and the contact stress is then reduced. The vibration is reduced, so that the frictional wear condition of the bearing is greatly improved. In summary, the PVX cage bearing has the smallest root mean square value of vibration, followed by the CF30 cage bearing, and the PEEK cage bearing has the largest.

In addition, it can also be seen from Fig. 4 that the increasing trend of the root mean square value of the vibration of CF30 and PVX cage bearings gradually becomes slower as the speed and load increase, which indicates that the larger load and speed are conducive to the formation of the transfer film.

Simulation study of self-lubricating silicon nitride bearings under dry friction

Establishment of thermal coupling model for self-lubricating silicon nitride bearings

The 3D models of PEEK cage, CF30 cage, and PVX cage 6206 silicon nitride ceramic bearings were created using the software Solidworks and then imported into Abaqus for simulation studies of stress and temperature rise. The skinning option of Abaqus was used to simulate the transfer film formed inside the CF30 and PVX cage bearings, and the PEEK cage bearings were not skinned. The structured hexahedral meshing is implemented for each part of the bearing with cell type C3D8RT and the membrane layer with M3D4 cell type, and its finite element meshing model is shown in Fig. 5.

Setting of simulation conditions

(1) Setting of material properties: The bearing ball

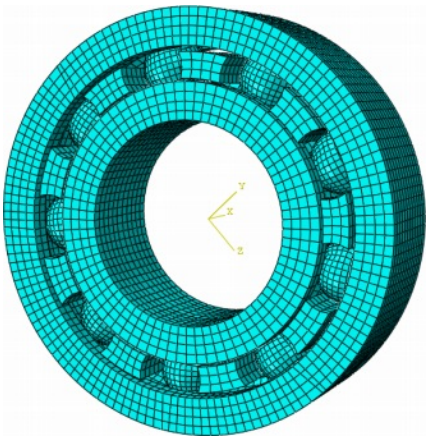

Fig. 5. Bearing meshing model.

and inner and outer ring are silicon nitride material, and the cage material and skin are set to PEEK, PVX and CF30 respectively, and the material properties are shown in Table 2.

(2) Setting of analysis step: The bearing display dynamics analysis is divided into 3 steps. The analysis step 1 is set to 0.001s to apply gravitational acceleration to the bearing as a whole and establish the contact relationship of each component; analysis step 2 is set to 0.001s to apply radial load to the inner ring; analysis step 3 is set to 0.01s to apply rotational speed to the inner ring.

(3) Bearing model contact settings: Set up face-to-face contact between the ball and inner and outer ring grooves and cage.

(4) Setting of boundary conditions and loads: Couple the inner ring and cage to the bearing center, and set reference points 1 and 2 respectively constrain the 6 degrees of freedom of the outer ring, apply radial load and rotational speed to the inner ring, radial load is 400N, 900N, 1750N, and rotational speed is 6000 r/min, 8000 r/min, 10000 r/min respectively.

Simulation results and analysis

Bearing stress analysis

At 8000 r/min - 900N, Fig. 6. compares the stress magnitude of the ball and inner and outer rings of PEEK cage bearings, CF30 cage bearings, and PVX cage bearings.

From Fig. 6, it can be seen that the stress value of the ball in each part of the 6206 silicon nitride bearing is the largest, followed by the outer ring, and the inner ring is the smallest. This is because under the action of centrifugal force, the contact force between the ball and the outer ring is greater, so the stress is also greater. From Fig. 6(a)-(c), (d)-(f), (g)-(i), it can be seen that the formation of transfer film can effectively reduce the stress of the bearing, this is because the transfer film material is softer than the silicon nitride material and the elastic modulus is much smaller than the silicon nitride material, so when the ball is in contact with the transfer film, the deformation-load coefficient becomes larger, so it is known from Equation (6) that the contact deformation becomes larger when the contact load is constant. The reduction of stress has a significant effect on increasing bearing life and reducing bearing wear. The effect of PVX transfer film is the most obvious, basically consistent with the test results analysis.

Table 4 compares the maximum stress values of the simulated and theoretical analysis results for PEEK, CF30, and PVX cage bearings at 8000 r/min - 900 N. It can be seen that the results are in good agreement,

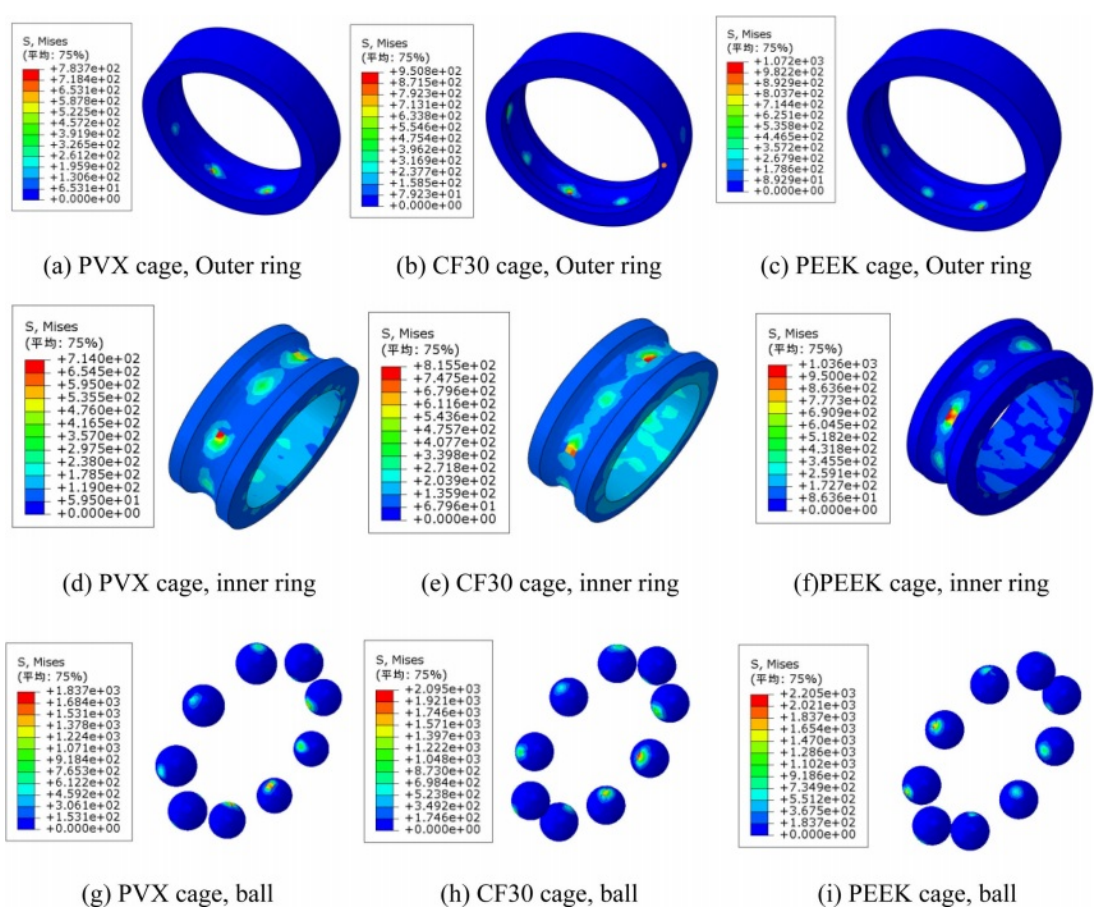

Fig. 6. Simulated stress values for PEEK, CF30, PVX cage bearing balls and inner and outer rings.

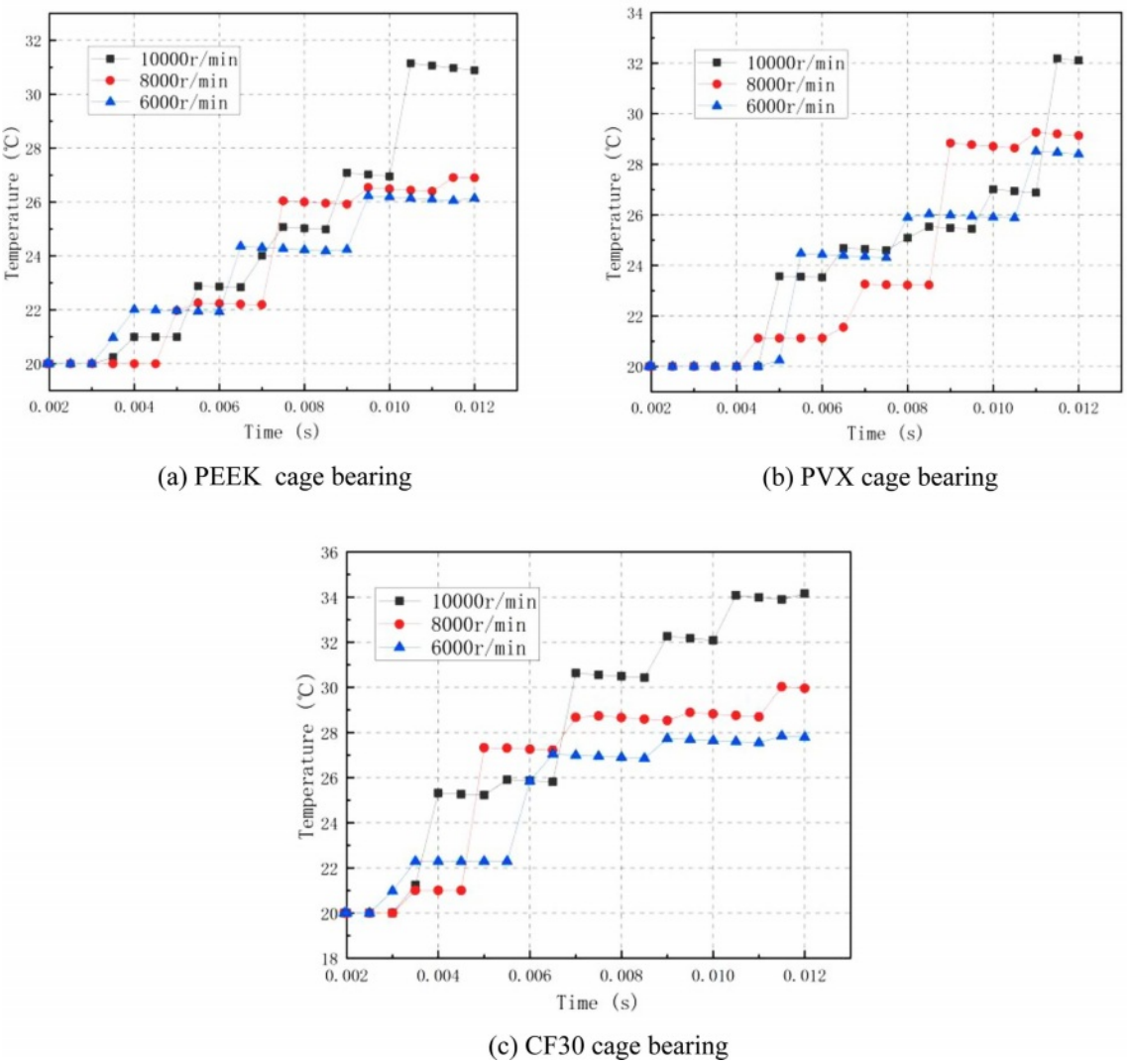

Fig. 7. Temperature rise curves of 3 types of bearings at different speeds at the same node.

indicating that the simulation model is more accurate.

Bearing temperature rise analysis

Given that the temperature sensor in the test is measured at 90° to the radial load in the outer ring, the temperature rise variation curve of the same position in the outer ring of the simulation model is plotted with node number N:3960, and the figure shows the temperature rise curves of PEEK, CF30 and PVX cage bearings at different speeds under 900N load. From Fig. 7, it can be seen that the temperature rises in a step-like manner, indicating that the temperature rise of the bearing is a dynamic process. Table 5 compares the simulation and test results under 900N radial load, and the values basically match, which also verifies the correctness of the simulation model.

Micro-physical analysis of PVX cage bearing after the test

Through the above analysis, it is known that the PVX cage bearing has the optimal service performance, so for the PVX cage bearing, the chemical composition of the transfer film is analyzed from a microscopic

Table 4. Comparison of calculated and simulated values of maximum stressin 3 types of bearings.

	PEEK cage bearings maximum stress (MPa)	CF30 cage bearings maximum stress (MPa)	PVX cage bearings maximum stress (MPa)
Simulation value	2205	2095	1837
Calculated values	2348.5	2182.7	1922.8
Relative Error	6.5%	4.2%	4.7%

Table 5. Comparison of temperature rise between test results and simulation results.

Rotational Speed (r/min)	PEEK cage bearing			CF30 cage bearing			PVX cage bearing		
	6000	8000	10000	6000	8000	10000	6000	8000	10000
Test results (°C)	26.4	28	30.6	27	30	34	27.4	29.4	32
Simulation results (°C)	26.3	26.9	31.1	27.8	29	34.1	28.5	29.3	32.2

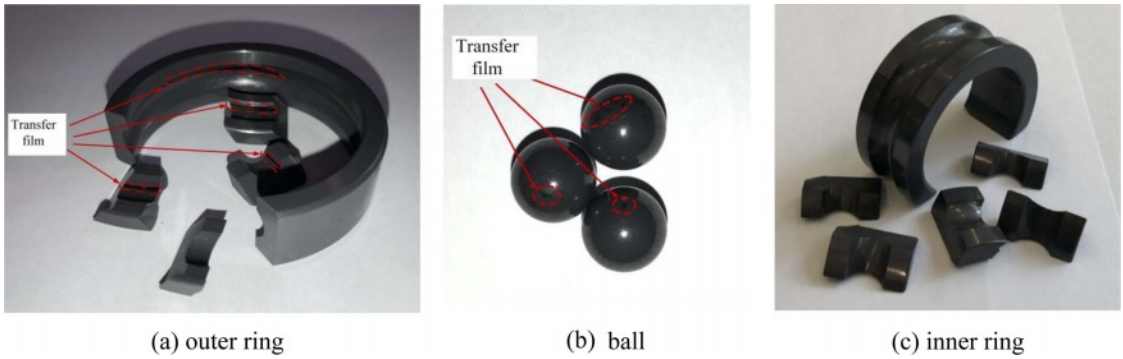

Fig. 8. Macro surface shape of inner and outer ring and ball of PVX cage bearing after test.

perspective to reveal its generation mechanism and further analyze the influence of the transfer film on the frictional wear of the bearing. The tested bearing was disassembled and cut non-destructively, and no obvious damage was observed in the contact area of the knife bearing. Meanwhile, as shown in Fig. 8, there existed black transfer film visible to the naked eye on the outer ring groove and ball surface, while no obvious transfer film was seen on the inner ring groove surface.

Scanning electron microscope (Hitachi S-4800, SEM) was used to examine the outer ring groove and ball of the bearing microscopically, Fig. 9 shows the SEM image of the outer ring groove and ball surface. From Fig. 9(a), it can be seen that the film is uniformly distributed on the outer ring groove surface in the shape of "fish scale", and there are also broken carbon fibers and block graphite above it. The cage wear chips cut down by the plowing action of the ball are thrown

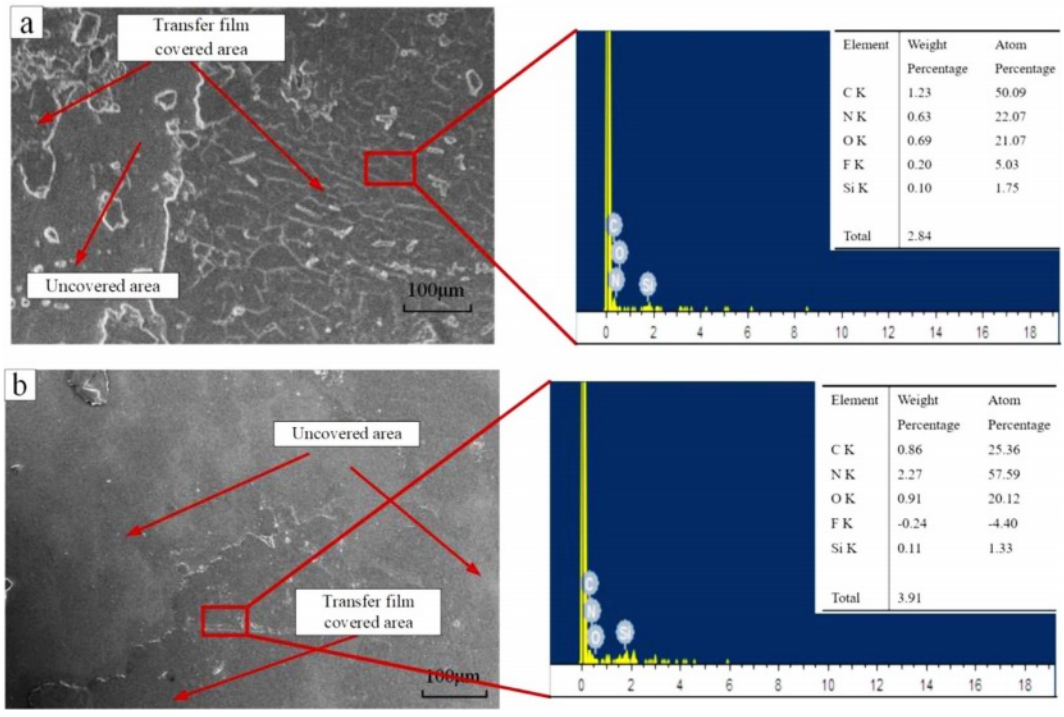

Fig. 9. SEM image and EDS image of outer ring and ball surface of PVX cage bearing after test (a) outer ring groove surface (b) ball surface.

onto the outer ring groove under centrifugal force and compacted under vertical load and cyclic stress, forming a uniform and continuous transfer film adhering to the outer ring groove surface, which has low shear stress [31]. In contrast, the area covered by the transfer film on the ball surface in Fig. 9(b) is small and discontinuous, indicating that the transfer film is poorly bonded to the ball. From the EDS diagram in Fig. 9, it can be seen that the main constituent elements of the transfer film are C and O. The outer ring transfer film also contains a small amount of element F, which is similar to the elemental composition of the PVX material, so these surface film layers are transferred from the cage to the outer ring groove and the ball surface. However, all areas in Fig. 9(a) and (b) are not damaged, which indicates that the transfer film effectively protects the friction surface and has the effect of wear reduction and lubrication to the bearing.

Conclusion

Stress-strain and friction torque analyses were performed on silicon nitride deep groove ball bearings subjected to radial loads under transfer film lubrication. Using a bearing life testing machine, a test and simulation study was conducted on PEEK, CF30, and PVX cage bearings under dry friction conditions. After the test, the PVX cage bearing with the best performance in service was analyzed for surface morphology, and the reliability of cage lubrication was verified. The following conclusions were drawn.

(1) Through the theoretical analysis it is known that when the deep groove ball bearing is subjected to radial load, there exists a limit angle to divide the bearing into the loading area and non-loading area. In addition, when the cage lubricated bearing is in operation, groove and ball surface will form a layer of polymer material transfer film, therefore, when the theoretical analysis is performed, the impact of the transfer film is needed, at this time, the ball does not contact with the groove directly, need to substitute the transfer film layer material elastic modulus, elastic hysteresis loss factor, etc. So the transfer film layer's existence reduces the stress of the silicon nitride deep groove ball bearing but will increase the friction torque M_E and M_C.

(2) Through the bearing dry friction test, we know that the bearing temperature rise in the non-loading area is not greatly affected by radial load, and is proportional to the speed, CF30 and PVX cage bearing will form a transfer film inside the bearing, making them slightly higher than the temperature rise of PEEK cage bearings; at the same time, the three bearing vibration root mean square value axis is proportional to the speed and radial load, the three bearing vibration root mean square value of the relationship between the size of: PEEK cage bearings > CF30 cage bearings > PVX cage bearings.

(3) The simulation software was used to establish a model of silicon nitride full ceramic ball bearing with transfer film lubrication, and the simulation and theoretical analysis results of the maximum stress value were compared, and the obtained temperature rise simulation results were found to be in basic match with the test results, which verified the correctness of the simulation model.

(4) After the test, the PVX bearing was cut and modified non-destructively to observe the morphology of the groove and ball surface. The results showed that there was a continuous and large area covered by transfer film in the groove of the outer ring of the bearing, and the area covered by transfer film on the ball surface was small. It was also found that there was no obvious damage to the transfer film covered and non-covered areas of the bearing contact surface, which indicated that the transfer film effectively protected the bearing and played the role of wear reduction and lubrication at the same time. The bearing supplies the transfer film by sacrificing the cage material, so it is critical to form an effective transfer film through low wear of the cage to ensure that the bearing will not fail due to excessive wear of the cage.

Acknowledgements

The authors acknowledge the collective support granted by the National Natural Science Foundation of China (Grant No 52105196), the Education Department of Liaoning Province (Grant No LJKMZ20220936), Young and Middle-aged Innovation Team of Shenyang (Grant No RC210343). National defense science and technology innovation zone plan: ultra-high precision ceramic bearing (No. 20-163-00-TS-006-002-11).

References

1. H. Wen, J. Sun, and W. Chen, Int. Mater. Rev. 29 (2015) 6-14.
2. M. Cao, X. Jin, and L. Chen, J. Ceram. Process Res. 4 (2021) 377-385.
3. W. Zhang, X. Chen, and S. Yamashita, ACS Appl. Nano Mater. 4 (2021) 3159-3166.
4. Z. Li, Y. Wang, and X. Cheng, ACS Appl. Mater. Interfaces 10 (2018) 2965-2975.
5. N. Kovalev, Myshkin, Friction. 6 (2018) 143-155.
6. M.D. Placette, S. Roy, D. White, S. Sundararajan, and C.J. Schwartz, Wear. 426-427 (2019) 1345-1353.
7. Y. Qi, J. Gong, W. Cao, and W. Honggang, J. Wuhan Univ. Technol. Mater. Sci. Ed. 35 (2020) 87-98.
8. A. Wang, S. Yan, and B. Lin, Friction. 5 (2017) 414-428.
9. J. Ma, X. Qi, and Y. Dong, Tribol. Int. 120 (2018) 233-242.
10. L. Guo, G. Zhang, and D. Wang, Composites, Part A. 102 (2017) 400-413.
11. G. Theiler and T. Gradt, Wear. 269 (2010) 278-284.
12. G. Jintang, Wear. 245 (2000) 100-106.

13. H. Koike, K. Kida, K. Mizobe, X. Shi, S. Oyama, and Y. Kashima, Tribol. Int. 90 (2015) 77-83.
14. H. Hyuga, M.I. Jones, K. Yoshida, N. Kondo, K. Hirao, and H. Kita, J. Ceram. Process Res. 10 (2009) 367-372.
15. Y. Lu, J. Yang, and J.Q. Gao, J. Ceram. Process Res. 9 (2008) 657-660.
16. S.H. Ahn and K.W. Nam, J. Ceram. Process Res. 17 (2016) 1046-1051.
17. H. Xin, H. Shi, W. Chen, J.H. Jia, W.L. Yang, and Z.M. Jin, Ceram. Int. 45 (2019) 6296-6302.
18. Z. Xia, Y. Wu, T. Ma, Z. Bao, J. Tian, J. Sun, and S. Li, Tribol. Int. 175 (2022) 107849.
19. M. Yakout, M.G.A. Nassef, and S. Backar, J. Mech. Sci. Technol. 33 (2019) 2037-2042.
20. M. Yakout, A. Elkhatib, and M.G.A. Nassef, J. Mech. Sci. Technol. 32 (2018) 91-99.
21. F.B. Oswald, E.V. Zaretsky, and J.V. Poplawski, Tribol. Trans. 55 (2012) 245-265.
22. E.V. Zaretsky, in "Rolling bearing life prediction, theory, and application" (Glenn Research Center Press, 2013) p. 8.
23. B. Fang, J. Zhang, J. Hong, and K. Yan, Lubricants. 11 (2023) 44.
24. S.J. Ma, Y.J. Yin, B. Chao, K. Yan, B. Fang, and J. Hong, Int. J. Mech. Sci. 245 (2023) 108098.
25. W. Mingkai, K. Yan, Q. Tang, J. Guo, Y. Zhu, and J. Hong, Tribol. Int. 179 (2023) 108163.
26. J. Wang, H. Zhao, and J. Li, J. Hunan Univ. Sci. Ed. 40 (2013) 46-51.
27. G. Colas, A. Saulot, Y. Michel, T. Filleter, and A. Merstallinger, Lubricants. 9 (2021) 38.
28. S. Von Goeldel, T. Reichenbach, F. König, L. Mayrhofer, G. Moras, G. Jacobs, and M. Moseler, Tribol. Lett. 69 (2021) 1-16.
29. S. Deng, X. Li, J. Wang, and H. Teng, Chin. J. Mech. Eng. 47 (2011) 114-120.
30. G. Yao, W. Wang, and J. Shen, Mater. Sci. Technol. 26 (2018) 59-65.
31. Y. Zhu, J. Chen, L. Jiang, and H. Wang, Runhua Yu Mifeng. 40 (2015) 61-64.
32. S. Bahadur, Wear. 245 (2000) 92-99.